Journal of the European Ceramic Society **18** (1998) 221–227

PII: S0955-2219(97)00118-0
0955-2219/98/$19.00 + 0.00

Subcritical Crack Propagation under Cyclic and Static Loading in Mullite and Mullite–Zirconia

C. K. L. Davies,[a] F. Guiu,[a] M. Li,[a] M. J. Reece,[a]* and R. Torrecillas[b]

[a]Department of Materials, Queen Mary and Westfield College, Mile End Road, London E1 4NS, UK
[b]Instituto Nacional del Carbon, Oviedo, Spain

(Received 28 January 1997; accepted 16 June 1997)

Abstract

The subcritical crack growth behaviour, under both static and cyclic loads, is examined in pure mullite and in a mullite—zirconia composite. It is found that in both materials the crack growth is influenced by the humidity of the testing environment. The crack growth rate dependence on the maximum stress intensity factor in the pure mullite is the same for static and cyclic loading. The presence of monoclinic zirconia particles in the mullite matrix in a ceramic composite enhances the crack growth resistance and produces faster crack growth rates occur under cyclic loading compared to static loading. These results, supported by the microstructural examination of crack profiles and fracture surfaces, are explained in terms of the interaction between the stress field of the zirconia particles and the cracks. © *1997 Elsevier Science Limited.*

Introduction

Many monolithic ceramic materials can experience some form of mechanical degradation when they are subjected to cyclic loads. This effect is manifested by a shorter time to failure and a faster growth rate of subcritical cracks than is experienced under static loads of the same magnitude.[1–3] These cyclic fatigue effects occur whenever strain irreversibilites occur in the loading–unloading cycles and there is good evidence to believe that these irreversibilities are due to the topological mismatch closure of the crack faces and microcracking around the crack tip.[2,4] The presence of grain boundaries, intergranular fracture and residual stresses always help to produce irreversible deformation and it is to be expected that in the ceramics with complex microstructures there will always be mechanisms available to produce mechanical cyclic fatigue effects. This seems to be in agreement with the observations that glasses and ceramics in which the cracks produce flat and smooth fracture surfaces do not seem to experience cyclic fatigue.[5,6]

In this paper we present the results of experiments on the static and cyclic crack growth behaviour in pure mullite and in mullite containing dispersed zirconia particles, with the purpose of examining and understanding the effect which the presence of stressed dispersed particles has on the existence to subcritical crack growth under both cyclic and static loads.

Materials and Specimens

The mullite specimens were produced from a commercially available powder (Bailkowski SA 193 CR) with an average particle size of 2·7 μm. The powder was spray dried, initially pressed at 40 MPa, and isostatically pressed at 200 MPa into blocks of $50\times50\times10\,mm^3$. The blocks were fired at 1750°C for 5 h and subsequently at 1450°C for another 5 h in order to reduce the amount of glassy phase. The microstructure of the mullite obtained [Fig. 1(a)] shows equaixed grains with an average size of 4 μm and elongated grains with an aspect ratio of 4. The porosity of the material was less than 3%, and a silica rich glassy phase was present at triple points extending along the grain boundaries.

Zircon powder (Ceraten S. A. Spain) with an average particle size of 1 μm and α-alumina powder (CT 3000 SG Alcoa RFA) with an average particle size of 0·5 μm were used to produce mullite-zirconia specimens by reaction sintering. The powder mixture was milled for two hours in isopropyl alcohol using alumina balls. The powder obtained was atomized into spherical aggregates of

*To whom correspondence should be addressed.

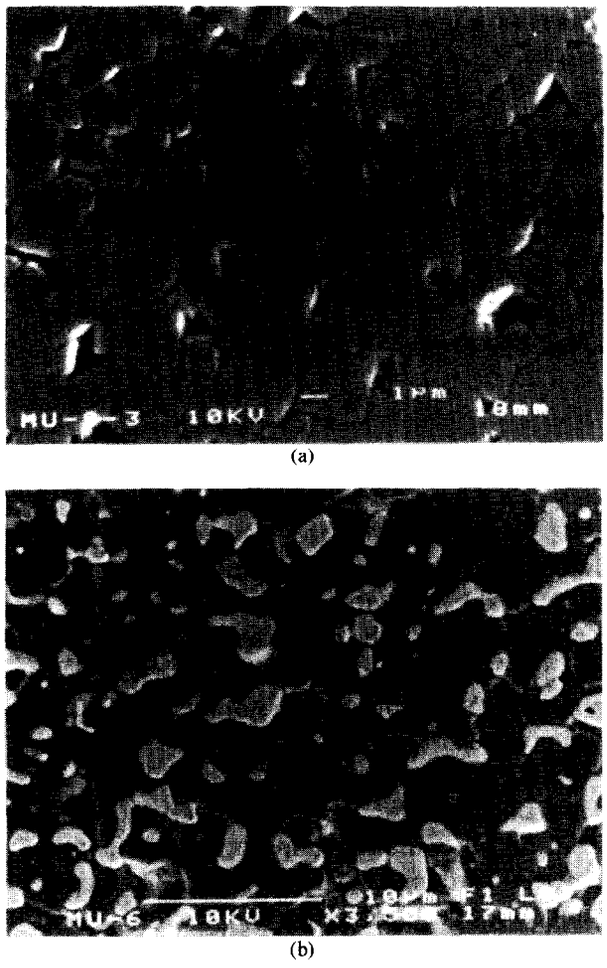

Fig. 1. SEM micrographs of polished, thermal etched specimens: (a) the mullite specimen and (b) the mullite–zirconia specimen.

between 50 and 150 μm diameter which was then isostatically pressed at 200 MPa into blocks and fired at 1600°C for 4 h. The microstructure of the material obtained consisted of four phases: mullite grains (of 4 μm average grain size); near spherical zirconia grains (between 1 and 2 μm); and small amounts of zircon and alumina [Fig. 1(b)]. The area fraction of, randomly distributed, zirconia particles was 18% and X-ray analysis showed that 90% of the zirconia particles had the monoclinic structure. This indicated that most of the zirconia grains had transformed to the monoclinic structure on cooling from the sintering temperature, as would be expected due to the absence of any stabilizing element in the original powder.

Double cantilever beam type specimens, of the dimensions shown in Table 1, were machined from the blocks of mullite and mullite-zirconia. The specimens were polished, notched and pre-cracked by forcing a wedge, in a controlled manner, into the notch.

The tests were carried out in a servo-hydraulic machine and the measurements reported in the results were started when the cracks had grown to a normalized length of 0·3. The crack lengths were monitored and measured during the tests with a long distance microscope with a resolution of 2 μm. However, when the crack growth rate was higher than 10^{-5} m s^{-1}, and too fast to be measured by this method, the crack length was calculated from a recorded plot of notch-opening displacement against time. The notch opening displacement was measured with a capacitance transducer, which was also used to obtain plots of load-notch displacement curves at intervals during the tests.

Three specimens of each material (labelled M for mullite and MZ for mullite-zirconia) were tested, always following a similar sequential loading procedure. The tests were started with cyclic loading at a frequency of 10 Hz and a load ratio of $R=-1$. When the crack growth rate had reached about 10^{-6} m s^{-1}, the load was reduced to slow down its propagation rate and the loading mode was changed from cyclic to static. The specimens M-1 and MZ-1 were cyclically and statically loaded in air with a relative humidity of 50% until the cracks had reached a length of a/w = 0·48. The tests were terminated to save the specimens for the examination of crack paths. The specimens M-2 and MZ-2 were fractured having reached the unstable crack growth stage while growing under static load. The specimens M-3 and MZ-3 were initially tested in air, and half way through the static loading sequence they were tested in an environment of N_2, with a relative humidity of less than 5% humidity.

Results

Typical plots of load-notch opening displacement for both the mullite and mullite–zirconia specimens

Table 1. Geometries and dimensions of tested specimens

		Dimension (mm)					*Notch length* (a_n/w)	*Precrack length* (a_p/w)
Material	*Geometry*	*B*	*W*	*h*	*c*	ϕ		
Mullite-1	DCB	4·10	37·97	6·36	7·19	4·67	0·337	0·373
Mullite-2	DCB	4·02	37·96	6·23	7·13	4·49	0·120	0·257
Mullite-3	DCB	4·02	37·77	6·23	7·35	4·29	0·123	0·259
Mullite–zirconia-1	WOL	4·54	29·09	7·12	7·50	4·52	0·164	0·236
Mullite–zirconia-2	WOL	4·17	29·57	7·22	7·50	4·48	0·211	0·506
Mullite–zirconia-3	WOL	4·73	29·10	7·25	7·03	4·32	0·149	0·297

are shown in Fig. 2. It can be seen that the curves are almost completely reversible for mullite and they show a very narrow loop for the mullite–zirconia specimens. This shows that the frictional losses during the cyclic growth of cracks in these materials are negligible and that the opening and closing of the crack is almost ideally reversible.

The relaxed tensile compliance of the specimens at different crack lengths for both materials are, as shown in Fig. 3, equal to the calibrated compliances, obtained from experimental calibrations for a free crack. This indicates that the cracks in these materials are not bridged by any kind of ligaments, in agreement with the absence of large hysteresis loops in the plots of Fig. 2. This observation is useful to validate the method used to calculate the length of the cracks from the values of the measured compliance.

The logarithmic plots of crack growth rate against the stress intensity factor for cracks growing under different loading and environment conditions are shown in Fig. 4–7. The data has been fitted assuming a power-law dependence, $da/dt = AK^n$, where A and n are material constants and K is the stress intensity factor. The stress intensity factors were calculated using the available solution for WOL specimens, or the experimentally calibrated compliance function of Fig. 3(a), after correcting the displacements to the loading line, for the DCB specimens.

The plots of Fig. 4 shows that in the mullite specimens (M-1 and M-2) the crack growth rate is similar for both static and cyclic loading at any value of the stress intensity factor. In other words, the material does not seem to be susceptible to any mechanical, cyclic fatigue effects, or degradation. The crack growth behaviour under static load in air, over a wider range of growth rates, is also shown in Fig. 4. It can be seen that there are three stages of crack growth and the slope of the plot of log(da/dt) against log(K_I) decreases sharply from region I ($n = 60$) to region II ($n = 7$). The effect of the N_2 environment on static fatigue crack growth for mullite specimen (M-3) is shown in Fig. 5, where the crack growth rates in air and in N_2 can be compared. Crack growth rates are slower in the low humidity environment for the same value of K_I, and the inflection in the plot, corresponding to stage II, occurs at much slower crack growth velocities (2×10^{-5} m s^{-1} in air, and 2×10^{-7} m s^{-1} in N_2).

The observed crack growth behaviour of mullite is typical of crack growth assisted by environmental corrosion effects, as reported in silica glass and alumina ceramics[7–9] for which it is suggested that chemical reaction with water helps to break the strained Si–O bonds at the crack tip.[9] The three regions of the V–K curves result correspond to a different rate-controlling mechanism of environmentally assisted crack growth. In region I the crack growth behaviour depends on both the stress intensity factor and the activity of water (relative humidity) in the environment. In region II the crack growth rate is mainly controlled by the rate of transport of water from the environment to the crack tip. This is the reason why the crack growth rate was approximately 100 times lower in N_2 than in air in this investigation. In region III the crack growth is independent of the humidity in the environment, so that specimens fractured at similar values of K_{Ic} under the different test humidities.

The crack growth rates against K_I in mullite–zirconia specimens (MZ-1 and MZ-2) under both cyclic and static loads are shown in Fig. 6. It can be seen that in this material, cyclic loads produce faster crack growth rates than static loads of the same

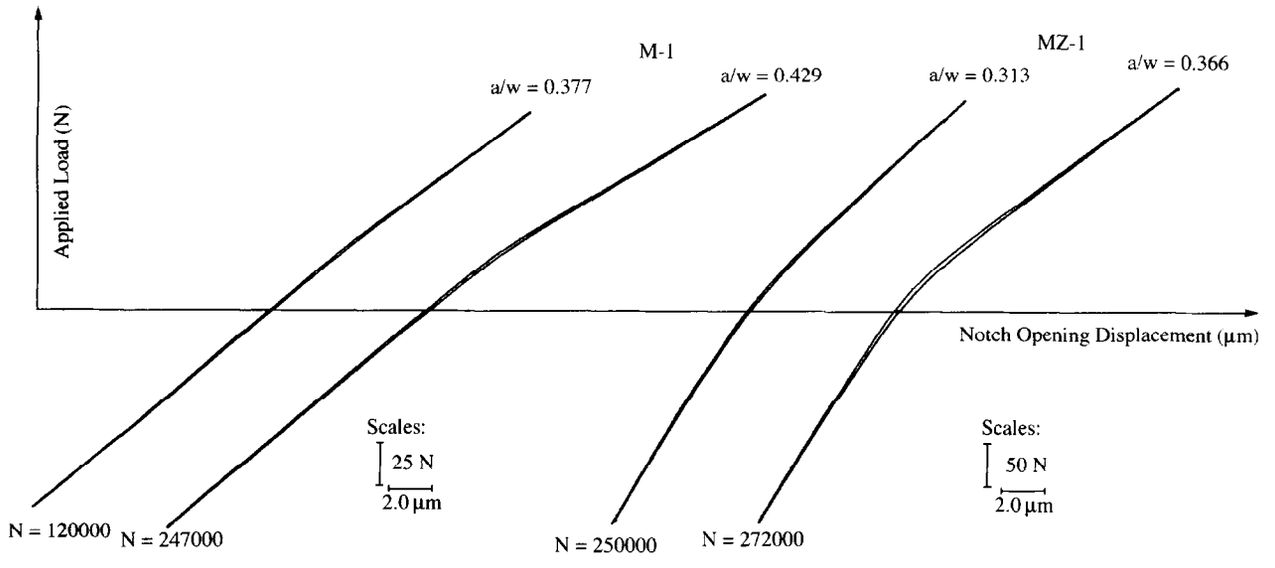

Fig. 2. Recorded applied load-notch opening displacement curves at different crack lengths under cyclic loading condition ($R = -1$) for the mullite and the mullite–zirconia specimens (the corresponding crack lengths and number of cycles are indicated in the plots).

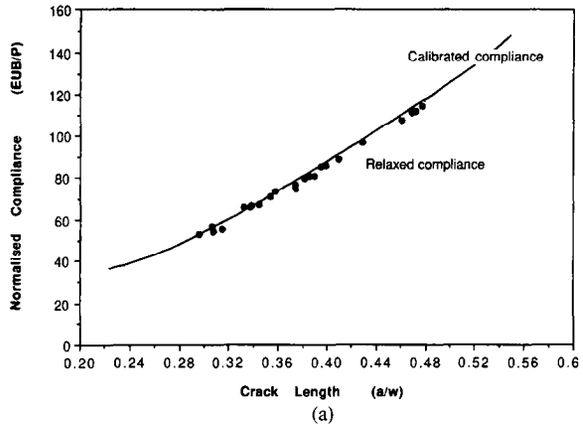

Fig. 3. Calibrated and measured compliances at different crack lengths for (a) the mullite specimen and (b) the mullite–zirconia specimen.

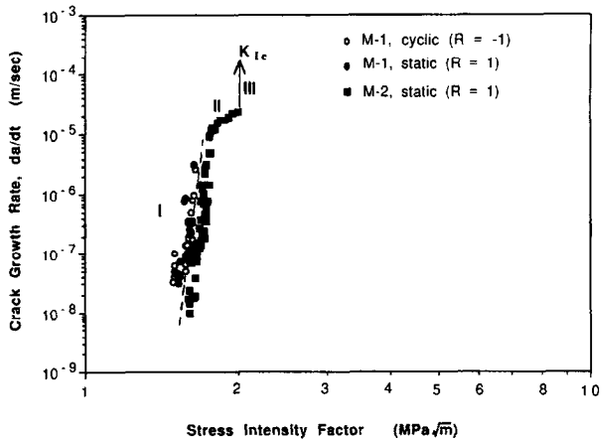

Fig. 4. Plots of crack growth rate against the maximum applied stress intensity factor under cyclic ($R=-1$) and static ($R=1$) loading conditions for the mullite-1 and mullite-2 specimens.

maximum value of K_I, and on effects of cyclic fatigue is clearly revealed. At the same time comparing the results of Fig. 6 with those of Fig. 4 for mullite, it can be seen that the addition of zirconia to mullite has increased the crack growth resistance and the fracture toughness, as measured by the value of K_{Ic} at the point of unstable crack propagation.

Figure 6 also shows three stages of crack growth rate under static load in air in mullite-zirconia. The

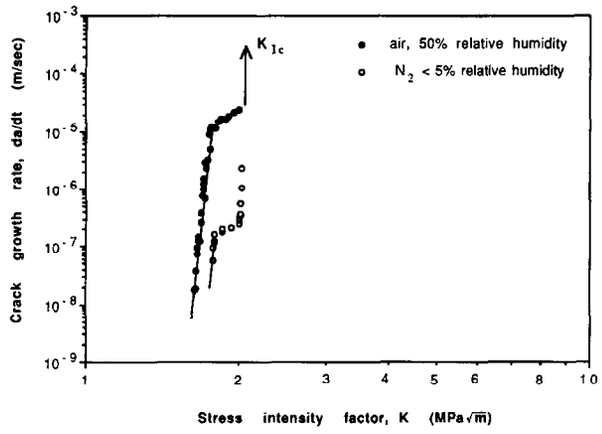

Fig. 5. Plots of crack growth rate against the maximum applied stress intensity factor under static ($R=1$) loading condition for the mullite-3 specimen tested in air and N_2 gas.

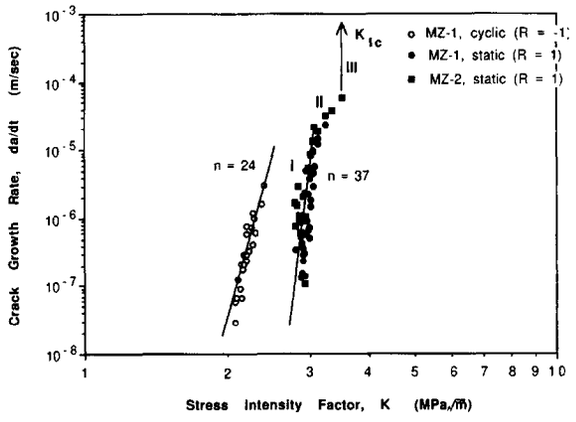

Fig. 6. Plots of crack growth rate against the maximum applied stress intensity factor under cyclic ($R=-1$) and static ($R=1$) loading conditions for the mullite–zirconia-1 and the mullite–zirconia-2 specimens.

effect of the environment is shown by the results plotted in Fig. 7, where it is apparent the slower crack growth rate of cracks in N_2 and the presence of stage II at lower rates. These results revealed crack growth in mullite-zirconia is also assisted by environmental corrosion effects, as explained in mullite.

The crack paths and the fracture surfaces of both mullite and mullite–zirconia specimens were examined under the SEM after the tests. The fracture surfaces for both materials contained fracture debris. In the mullite, the crack surfaces were transgranular and flat (Fig. 8), with very little undulation, and with a small residual crack opening, which made the crack visible without the need to wedge the crack open (Fig. 9).

The fracture surfaces of the mullite-zirconia specimens were also predominantly transgranular but were rougher than those of the mullite (Fig. 10). The crack path in this material had short range undulations, rather than sharp deflections, that appeared to be produced by interaction of the crack with the zirconia particles. A very large

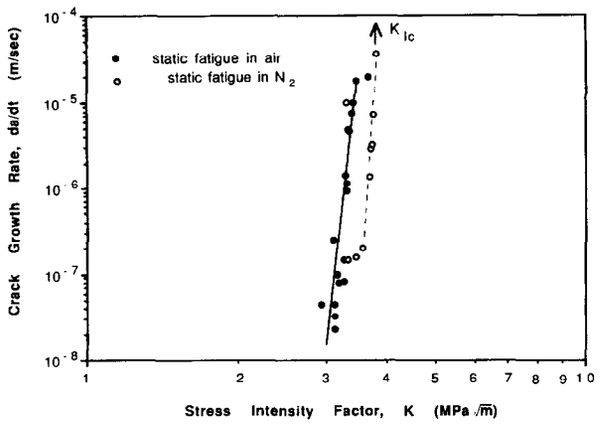

Fig. 7. Plots of crack growth rate against the maximum applied stress intensity factor under static ($R=1$) loading condition for the mullite-3 specimen tested in air and N_2 gas.

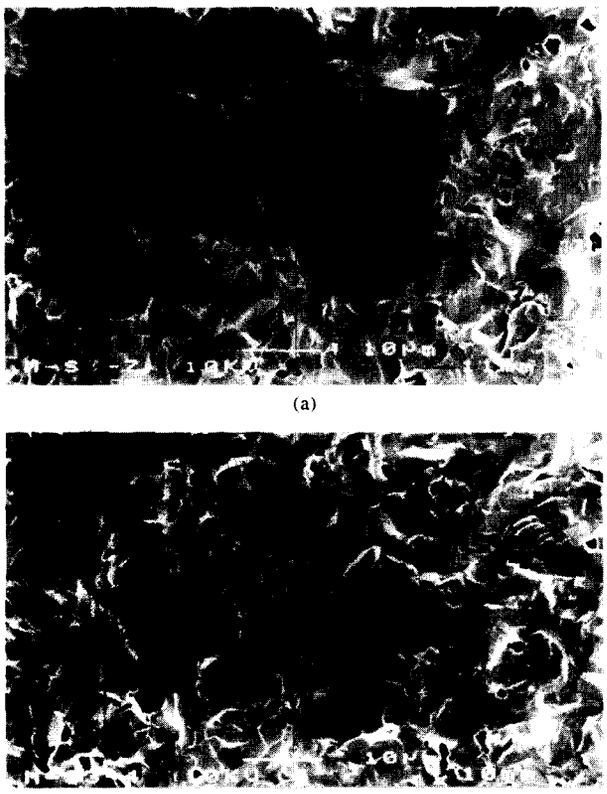

(a)

(b)

Fig. 8. SEM micrographs of fracture surfaces of the mullite specimen showing transgranular failure: (a) static and (b) cyclic.

number of these particle were intersected by the crack (Fig. 11).

Discussion

The observations of the effect of environment on the rate of crack growth under static loads strongly suggest that the subcritical crack growth in both mullite and mullite-zirconia is assisted by the corrosive effects of the water vapour in the test environment, very much like the effect of water on silica glass and zirconia.[9,10] This is not unexpected due to similar Si–O bonding in mullite and silica. Hence, the crack path through the mullite grains is not influenced by the presence of silica in the grain boundaries and a transgranular failure is obtained with features similar to that of glass.

The relatively simple mode of crack propagation in mullite, and the absence of any residual stresses, make this material insensitive to the unloading sequences during cyclic loading, and therefore, as shown in Fig. 4, there is no cyclic fatigue effect upon the rate of crack growth.[11] In other words, there is no mechanism of cyclic fatigue available in this material to produce enhanced crack growth, as is also suggested by the reversible loading-unloading behaviour observed in the plots of load-crack opening displacement of Fig. 2.

If crack growth is controlled by the same mechanism under static and cyclic loading conditions, the cyclic crack growth rate can be calculated by integration of the static crack growth velocity over the span of a fatigue cycle for the region where the relation $da/dt = AK_I^n$ is satisfied. If the value of $n=60$ is used for the static plot the calculation predicts a cyclic crack growth rate shown as a broken line in Fig. 4, which is within the scatter of the experimental cyclic results.

The subcritical crack growth in mullite-zirconia under static load is also environmentally controlled, as in mullite, but it is also influenced by the presence of the zirconia particles. These particles,

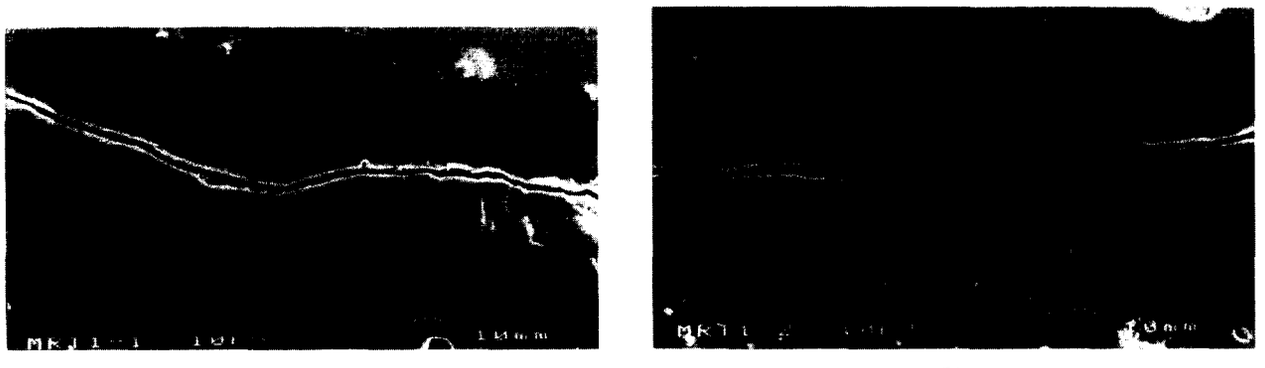

(a) (b)

Fig. 9. Fatigue crack path of the mullite specimen behind the crack tip showing straight feature: (a) 3·9 mm and (b) 2·3 mm.

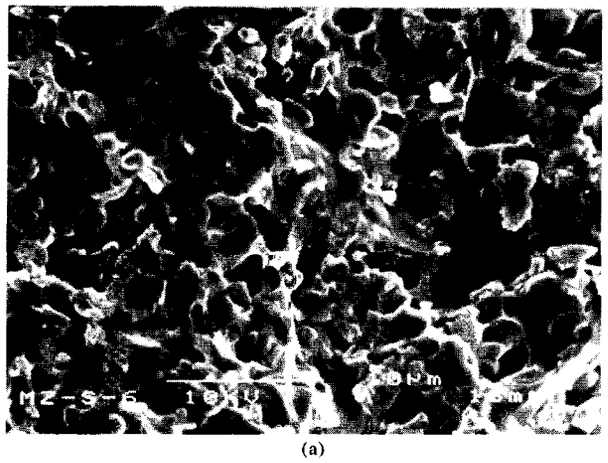

(a)

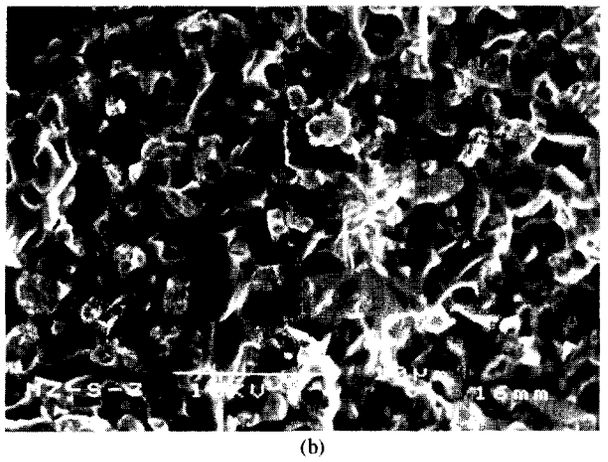

(b)

Fig. 10. SEM micrographs of fracture surfaces of the mullite–zirconia specimen showing transgranular failure: (a) static and (b) cyclic.

having transformed to the monoclinic phase during cooling from the sintering temperature, are under a state of stress with a hydrostatically compressive component, and the cracks interact with this internal stress. This interaction is such that a crack growing in the mullite matrix is attracted towards a compressed particle, and this can induce the short range undulations observed in the crack paths of this material. If the crack moves into the particle, and intersects it, as seen in micrograph of Fig. 11, it experiences a negative stress intensity factor produced by the hydrostatic compressive field. A similar effect is experienced by the wake if the crack moves through the mullite matrix between transformed particles.[12] All these effects must result in an overall increase in crack growth resistance and fracture toughness of the mullite–zirconia composite, as observed in the present experiments.

The presence of residual stresses and the undulations in the crack path, make the load-crack opening behaviour in mullite–zirconia less reversible than it is in mullite, as revealed in Fig. 2, and this makes the material more susceptible to the effects of load reversals and therefore cyclic fatigue effects. It has already been argued elsewhere, that mismatch of the crack faces, residual stresses, or both, can help the extension of a crack under reversed loading by mechanical effects which act independently of environmental considerations.[11]

The authors are aware that alternative explanations have been suggested for the toughening effect that transformed zirconia particles exert on other ceramics. In alumina-zirconia for example, microcracking produced in the matrix by the stress field around the particles, has been suggested as being responsible for the toughening.[13,14] However, the evidence to support this interpretation is not very compelling. Microcracking was never seen under SEM in the mullite–zirconia that we have tested, in spite of efforts made to detect them. In alumina–zirconia, they have been reported to be present in thin foils examined under TEM,[13] without proof that these cracks have not formed in the thinning process, as is most likely, to happen if the foils are internally stressed.

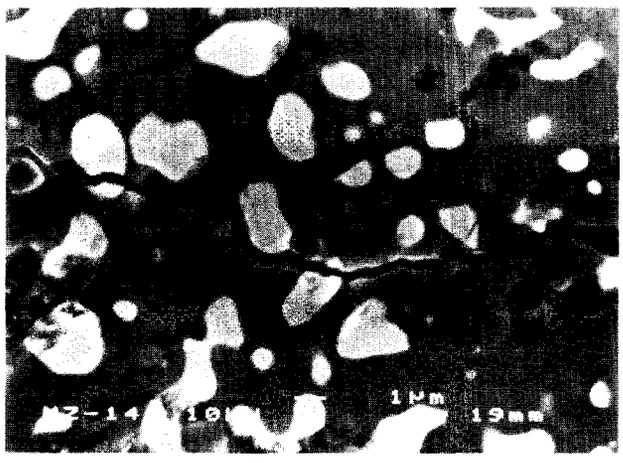

(a)

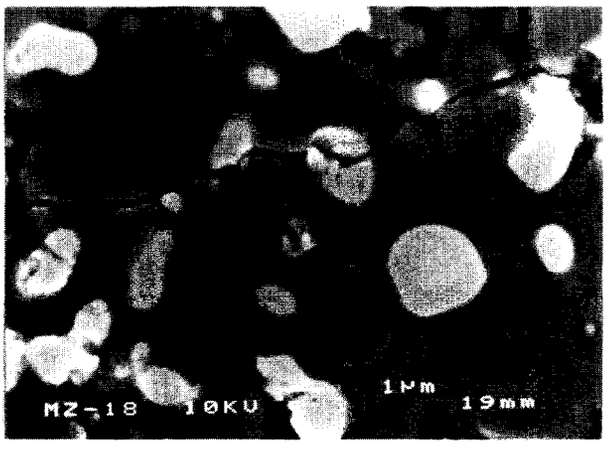

(b)

Fig. 11. Fatigue crack path of the mullite–zirconia specimen behind the crack tip showing that a very large number of zirconia particles were intersected by the crack: (a) 1·8 mm and (b) 0·8 mm.

The explanation that we have proposed for the behaviour of subcritical cracks, in both mullite and mullite–zirconia, is consistent with the experimental results and observations and the most plausible that can be offered on sound physical arguments.

Acknowledgements

This work was supported by the CEC under the Brite-EuRam initiative (BRE2-CT94-0613). We would like to thank G Fantozzi and C Olagnon from INSA, Lyon for their discussions.

References

1. Dauskardt, R. H., Yu, W. and Ritchie, R. O., *J. Am. Ceram. Soc.*, 1987, **70**, c-248.
2. Reece, M. J., Guiu, F. and Sammur, M. F. R., *J. Am. Ceram. Soc.*, 1989, **72**, 348.
3. Guiu, F., Reece, M. J. and Vaughan, D. A. J., *J. Mater. Sci.*, 1991, **26**, 3275.
4. Guiu, F., Li, M. and Reece, M. J., *J. Am. Ceram. Soc.*, 1992, **75**, 2976.
5. Evans, A. G. and Fuller, E. R., *Metallurgica Transactions*, 1974, **5**, 27.
6. Evans, A. G., *International Journal of Fracture*, 1980, **16**, 485.
7. Wiederhorn, S. M., *J. Am. Ceram. Soc.*, 1967, **59**, 407.
8. Evans, A. G., *J. Mater. Sci.*, 1972, **7**, 1137.
9. Wiederhorn, S. M., Freiman, S. W., Fuller, E. R. Jr and Simmons, C. J., *J. Mater. Sci.*, 1982, **17**, 3460.
10. Wakai, F., Sakuramoto, H., Sakaguchi, S. and Matsuno, Y., *J. Soc. Mater. Sci. Japan*, 1986, **35**, 898.
11. Li, M. and Guiu, F., *Acta Metall. Meter.*, 1995, **43**, 1859.
12. Li, J. M. C. and Sanday, S. C., *Acta Metall.*, 1986, **34**, 537.
13. Ruhle, A. G., Evans, R. M., Mcmeeking, Charalambides, P. G. and Hutchinson, J. W., *Acta Metall.*, 1987, **35**, 2701.
14. Stevens, R., *Zirconia and Zirconia Ceramics*, Magnesium Elektron Ltd, 1986.